ELSEVIER

Atmospheric Research 69 (2003) 73–97

ATMOSPHERIC RESEARCH

www.elsevier.com/locate/atmos

Microphysical and optical properties of aerosol particles in urban zone during ESCOMPTE

M. Mallet[a,*], J.C. Roger[b], S. Despiau[a], O. Dubovik[c], J.P. Putaud[d]

[a] *LEPI, Université de Toulon et du Var, France*
[b] *LOCL, Université du Littoral Côte d'Opale, France*
[c] *NASA/Goddard Space Flight Center, Greenbelt, MD, USA*
[d] *Joint Research Centre, Ispra, Italy*

Received 23 April 2003; received in revised form 10 July 2003; accepted 10 July 2003

Abstract

Microphysical and optical properties of the main aerosol species on a peri-urban site have been investigated during the ESCOMPTE experiment. Ammonium sulfate (AS), nitrate (N), black carbon (BC), particulate organic matter (POM), sea salt (SS) and mineral aerosol (D) size distributions have been used, associated with their refractive index, to compute, from the Mie theory, the key radiative aerosol properties as the extinction coefficient K_{ext}, the mass extinction efficiencies σ_{ext}, the single scattering albedo ω_0 and the asymmetry parameter g at the wavelength of 550 nm. Optical computations show that 90% of the light extinction is due to anthropogenic aerosol and only 10% is due to natural aerosol (SS and D). $44 \pm 6\%$ of the extinction is due to (AS) and $40 \pm 6\%$ to carbonaceous particles ($20 \pm 4\%$ to BC and $21 \pm 4\%$ to POM). Nitrate aerosol has a weak contribution of $5 \pm 2\%$. Computations of the mass extinction efficiencies σ_{ext}, single scattering albedo ω_0 and asymmetry parameter g indicate that the optical properties of the anthropogenic aerosol are often quite different from those yet published and generally used in global models. For example, the (AS) mean specific mass extinction presents a large difference with the value classically adopted at low relative humidity ($h < 60\%$) (2.6 ± 0.5 instead of 6 $m^2\ g^{-1}$ at 550 nm). The optical properties of the total aerosol layer, including all the aerosol species, indicate a mean observed single-scattering albedo $\omega_0 = 0.85 \pm 0.05$, leading to an important absorption of the solar radiation and an asymmetry parameter $g = 0.59 \pm 0.05$ which are in a reasonably good agreements with the AERONET retrieval of ω_0 ($= 0.86 \pm 0.05$) and g ($= 0.64 \pm 0.05$) at this wavelength.

Keywords: Aerosol; Aerosol number size distribution; Chemical composition; Aerosol optical properties; Climate change

* Corresponding author. Tel.: +33-4-94142446; fax: +33-4-94142572.
E-mail address: marc.mallet@univ-tln.fr (M. Mallet).

0169-8095/$ - see front matter © 2003 Elsevier B.V. All rights reserved.
doi:10.1016/j.atmosres.2003.07.001

1. Introduction

It is now clearly recognized that anthropogenic aerosol particles modify the climate through three well-known processes. Directly, by scattering the solar radiation back to space leading to a cooling effect, and (or) by absorbing the solar radiation leading to a heating effect (Haywood and Shine, 1997). Indirectly, by changing the clouds properties (Rosenfeld, 2000) when aerosol particles act as cloud condensation nuclei. Semi-directly, by favouring the evaporation of clouds when high concentration of absorbing aerosol as black carbon are present in the atmosphere (Ackerman et al., 2000).

However, while the radiative forcing due to greenhouse gases may be determined to a reasonably high degree of accuracy, the uncertainties relating to aerosol radiative forcings remain large (IPCC, 2001). This is due not only to the heterogeneous spatial and temporal distribution of tropospheric aerosol particles, their different origins (natural and anthropogenic), their physical and chemical behaviour in the free troposphere, but also to the lack of database related to optical and microphysical properties of the aerosol particles.

An improvement on the level of confidence on the aerosol radiative effect requires a full range of observations, including chemical (such as composition), physical (such as number and mass size distribution) and optical measurements of aerosol. These characteristics may be deduced from experiments in selected regions as the previous experiment, ACE1 (Bates et al., 1998), for clean aerosol in the minimally polluted Southern Hemisphere marine atmosphere or ACE2, TARFOX and INDOEX (Raes et al., 2000; Hartley et al., 2000; Ramanathan et al., 2001) for anthropogenic aerosol transported by wind from the European continent, the United States eastern seaboard and the Indian continent, respectively.

Among all the numerous sources of anthropogenic aerosol particles, the pollutant particles emitted in large urban areas are now clearly recognized as one of the most important and cities emerge as an important research topic in atmospheric chemistry and effect on climate. Indeed, pollutants emitted in the industrialised regions, mainly consisting of sulfate, nitrate, black carbon and particulate organic matter modify the albedo of the surface–atmosphere system, leading to a modification of the local or regional climate when pollutants are transported out of the source regions into surrounding areas. For example, a recent study realized by Raga et al. (2001) indicates that the presence of a pollution aerosol layer over a city reduces irradiation at the surface by 18% and increases the temperature into the boundary layer. Local experimental studies focused on the microphysical, chemical and optical aerosol properties are clearly required to better characterize the urban particles. These in situ observations should be also used as input in mesoscale models including urban source or in global models which the resolution is improving rapidly over time, and should be permitted to take into account urban emission, and estimate their climatic influence in the future.

In the frame of this problematic, the ESCOMPTE experiment (Cros et al., submitted for publication) allowed us to study the microphysical and optical properties of the main aerosol species: ammonium sulfate (AS), nitrate (N), black carbon (BC), particulate organic matter (POM), sea salt (SS) and mineral aerosol (D). Their size distributions measured in situ, associated with their refractive index, have been used to compute their optical properties from the Mie theory. We focused our computations on the key aerosol

optical properties generally used in radiative simulations, including the extinction coefficient K_{ext} (km^{-1}), the single scattering albedo ω_0, which represents the ratio of light scattering to scattering + absorption and determines the sign (cooling/heating, depending of the earth albedo) of the aerosol radiative forcing, the asymmetry parameter g, which represents the fraction of radiation scattered by aerosol and the extinction per unit mass of aerosol σ_{ext} (m^2 g^{-1}), which represents the extinction of aerosol per unit mass.

2. Experimental campaign and instrumentation

Between the 4th of June and the 13th of July 2001, the co-operative experiment ESCOMPTE (field experiments to constrain models of atmospheric pollution and transport of emissions) took place in the South of France, in the Marseille area (Cros et al., submitted for publication). Among the numerous objectives of this experiment, one concerned the physico-chemical characterisation of aerosol particles in urban and peri-urban zones. The results presented here are based upon a data set measured in the peri-urban zone of Marseille (''Vallon Dol'' Site, Fig. 1), mainly polluted by the traffic during 3 IOP corresponding to meteorological conditions favourable to pollution event.

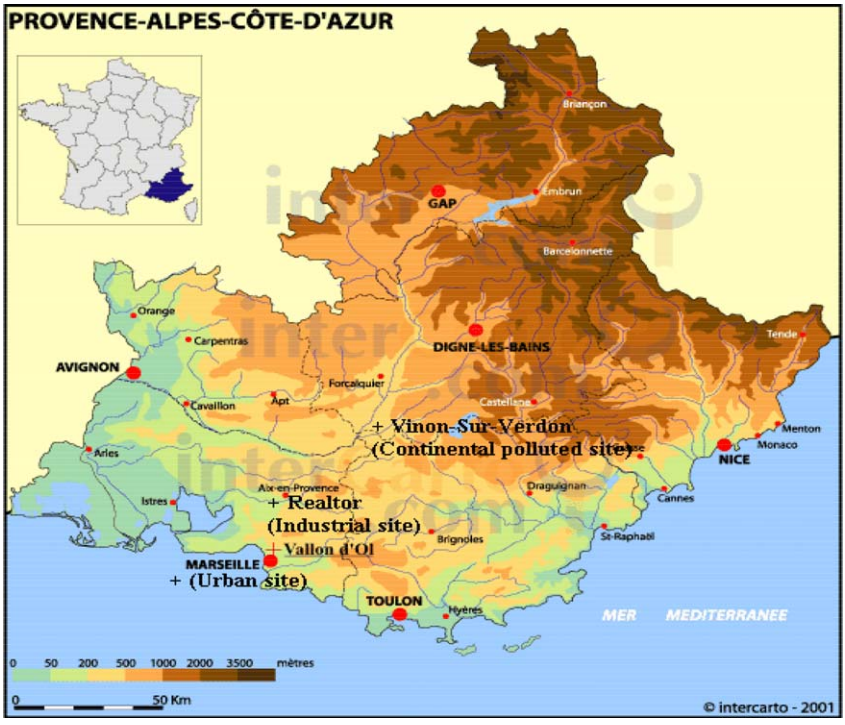

Fig. 1. The Vallon d'Ol Site in peri-urban zone of Marseille.

Size-segregated aerosol was collected at ambient relative humidity using a low-pressure 6-stage Berner impactor (LPI 80/0.05) loaded with pre-fired aluminum foils. The 50% aerodynamic cut-off diameters were 0.06, 0.125, 0.25, 0.5, 1, 2, 4 and 8 μm. According to Stern (1977), the impactor aerodynamic diameters d_{ae} were converted to geometric diameters, d_p, for each bin size and each chemical species. The sampling duration was about 8 h (1000 to 1800 h). Negative artifacts in impactors due to the volatilization of semi-volatile compounds at low pressure and to losses on impactor walls are generally $<4\%$ (Hering et al., 1997).

The mass of carbon collected on the aluminum foils was determined using a thermal method (Evolved Gas Analysis, EGA), where samples are exposed successively to five increasing temperature plateaus up to 650 °C in an oxygen-free carrier gas, and then in an oxygen-rich carrier gas at 650–750 °C (Putaud et al., 2000). The carbon evolved at $T<650$ °C in He is defined as OC but contains also carbonate, and the fraction evolved at $T>650$ °C in the oxidizing carrier gas is expected to be black carbon (BC). However, due to possible charring during the analysis, the BC values obtained with this routine method can be highly overestimated. Therefore, each sample was divided into two half foils, one of which was exposed at 340 °C for 2 h in an oxidizing carrier gas (He/O_2 80:20). This thermal treatment was shown to remove most of the OC susceptible to be charred (Cachier et al., 1989). The carbon fraction evolved from the treated aliquot at $T>650$ °C was defined as BC. The detector was calibrated twice a day by injecting known amounts of pure CO_2 and the instrument overall response checked daily using a sodium oxalate standard. The analytical precision is ± 8%, based on repeated measurements of the same sample. International intercomparison exercises showed that the overall uncertainties of TC (TC = OC + BC) and BC determinations are $<10\%$, and ca. 40% for TC and BC, respectively.

In the following calculation, instead of (OC), we will consider the particulate organic matter (POM) which includes in addition to carbon, hydrogen atoms, and minor amounts of other species. The mass of Particulate Organic Matter is computed from the mass of Organic Carbon as follows (Liousse et al., 1996):

$$\mathrm{POM} = 1.3 \times \mathrm{OC} \tag{1}$$

Na^+, NH_4^+, K^+, Mg^{2+}, Ca^{2+}, Cl^-, NO_3^-, SO_4^{2-} concentrations were measured by ion chromatography (IC). The precision of the measurements is ± 10% (Putaud et al., 2000).

They were used to calculate the total mass concentrations (noted M_i) of the main aerosol species but also the mass on each impactor stage allowing to estimate the mass size distributions of each component. Non-sea-salt Sulfate fraction (e.g., $nssSO_4^{2-}$) was derived using Na^+ as a sea salt tracer and a standard sea salt composition. Ammonium sulfate (AS) concentration was computed using the $nssSO_4^{2-}$ fraction associated with the ammonium NH_4^+. Nitrate (N) was deduced from the NO_3^- concentrations. Sea salt (SS) concentrations were calculated from the Na^+ concentrations, the ratio of K^+, Mg^{2+}, $Ca^{2+}$and $SO_2^{4}{}_-$ over Na^+ in standard seawater and the measured Cl^- concentrations to account for possible Cl^- depletion. Dust concentrations were estimated from the amount of non-sea salt Ca^{2+} measured in each impactor stage and the regression between non-sea salt Ca^{2+} and ash (considered as mineral dust) determined from co-located and simulta-

neous sampling on Whatman 41 ashless filters. The uncertainty in the slope of the regression between ash, measured in water extracted filters, and nssCa^{2+} (mineral dust = 5.7 × nssCa^{2+}) was ± 1.7 (95% confidence level).

All these analyses are made on each impactor stage, allowing us to obtain for the first time the mass size distribution of each component, and for the second time, the total mass concentration of each component (noted M_i) by summing the concentrations of each stage.

We used also a CE 318 automatic sun tracking photometer (manufactured by CIMEL Electronique, Paris). This instrument performed sky radiance and direct solar irradiance measurements over Marseille for the 440, 670, 870 and 1020 nm wavelenghts. The Angström coefficient (Angström, 1964), $\alpha_{440/670}$, is obtained from the optical thicknesses deduced from the channels at 440 and 670 nm. The Dubovik and King (2000) inversion algorithm allowed to retrieve the single scattering albedo (ω_0), and the asymmetry parameter (g) for the whole atmospheric column. Photometer measurements obtained between June 24 and July 04 are used in this study.

3. Method

The mass distribution deduced from concentrations measured on each impactor stage was fitted with a lognormal function from which the mass mode radius ($r_{g,m}$) and the standard deviation (σ) were retrieved. In order to use the theory of Mie (1908), the particles were assumed to be spherical and the "mass" ($r_{g,m}$, σ) parameters were transformed into "number" parameters ($r_{g,n}$, σ, N), for each component (i) according to Seinfeld and Pandis (1998) relations:

$$\log r_{g,n} = \log r_{g,m} - 3(\log\sigma)^2 \ln 10 \tag{2}$$

$$N_i = \sum_i 3M_i / 4\pi \overline{r_i^3} \rho_i \tag{3}$$

In relation (2), which is useful both for dry and wet states, the geometric standard deviation, σ, remains the same for the two distributions. In relation (3), M_i and ρ_i are the mass and the particulate density of the component (i) and $\overline{r_i}$ an equivalent radius defined by:

$$\overline{r_i^3} = r_i^3 \left(\frac{9}{2} \times \ln^2 \sigma_i \right) \tag{4}$$

It should be noted that the accumulation and the coarse mode of a mass size distribution correspond, after transformation, to the fine and the accumulation mode, respectively, of a classical number size distribution (Whitby, 1978).

Finally, to compute the complex refractive index for each component at the ambient relative humidity (h), n_h, we used the Hänel (1976) relations for an external mixture state at one wavelength λ:

$$n_h(\lambda) = n_{H_2O}(\lambda) + (n_0(\lambda) - n_{H_2O}(\lambda)) \left(\frac{r_{g,n(h)}}{r_{g,n(0)}} \right)^{-3} \tag{5}$$

Table 1
Relative humidity during ESCOMPTE

Date	h (%)
23/06	37.50
24/06	61.40
25/06	61.00
26/06	45.00
02/07	45.00
03/07	55.00
04/07	50.00
10/07	71.50
11/07	42.00

where n_{H2O} is the water refractive index and n_0, n_h are, respectively, the refractive index of the aerosol species studied in dry state and at ambient relative humidity. The number geometric radius in dry state $r_{g,n(0)}$ and at ambient humidity $r_{g,n(h)}$, are linked by the relation (Hänel, 1976):

$$r_{g,n(0)} = r_{g,n(h)}(1-h)^e \tag{6}$$

where h is the relative humidity. During ESCOMPTE, h varied between 37.5% and 71.5% (Table 1). The coefficient e depends on the considered type of aerosol. It is equal to 0.25 for POM (Chazette and Liousse, 2001) and 0.285 for AS, N and SS (Hänel, 1976). We assumed (BC) and (D) to be non-hygroscopic (thus $e=0$). Once we got the microphysical properties ($r_{g,n(h)}$, σ, N, $n_h(\lambda)$) for one component, we computed its optical properties ($K_{ext}(\lambda)$, $\omega_0(\lambda)$, $g(\lambda)$ and $\sigma_{ext}(\lambda)$) at 550 nm, using the Mie theory (1908).

4. Results

4.1. Microphysical and optical properties of each aerosol specie

The different parameters presented above are computed for each aerosol specie and grouped together in Tables 2 and 3.

4.1.1. Ammonium sulfate (AS)

The (AS) mass size distributions measured during IOPs are presented in Fig. 2. They are unimodal with a mode diameter and a standard deviation between 0.2–0.4 and 1.74 μm, respectively. The corresponding number geometrical radius $r^{AS}_{g,n(h)}$, at ambient humidity, is equal to 0.05 ± 0.01 μm (Table 2) with an associated standard deviation $\sigma = 1.74 \pm 0.07$. This leads to $r^{AS}_{g,n(0)}$ value equal to 0.040 ± 0.005 μm in dry state. (AS) is also mainly found on the fine mode by Zhuang et al. (1999) in a recent study in polluted urban zone.

On the basis of the water-soluble aerosol model (WCP, 1984), the complex refractive index used is $1.53-6.10^{-3}i$ at 550 nm, in dry state. The extinction coefficient vary from 0.015 to 0.043 km^{-1} and represents $44 \pm 6\%$ of the total light extinction at 550 nm. Hence, (AS) represents the major contributor to light extinction (Fig. 8) as it was found in different studies (Ramanathan et al., 2001; Hegg et al., 1997).

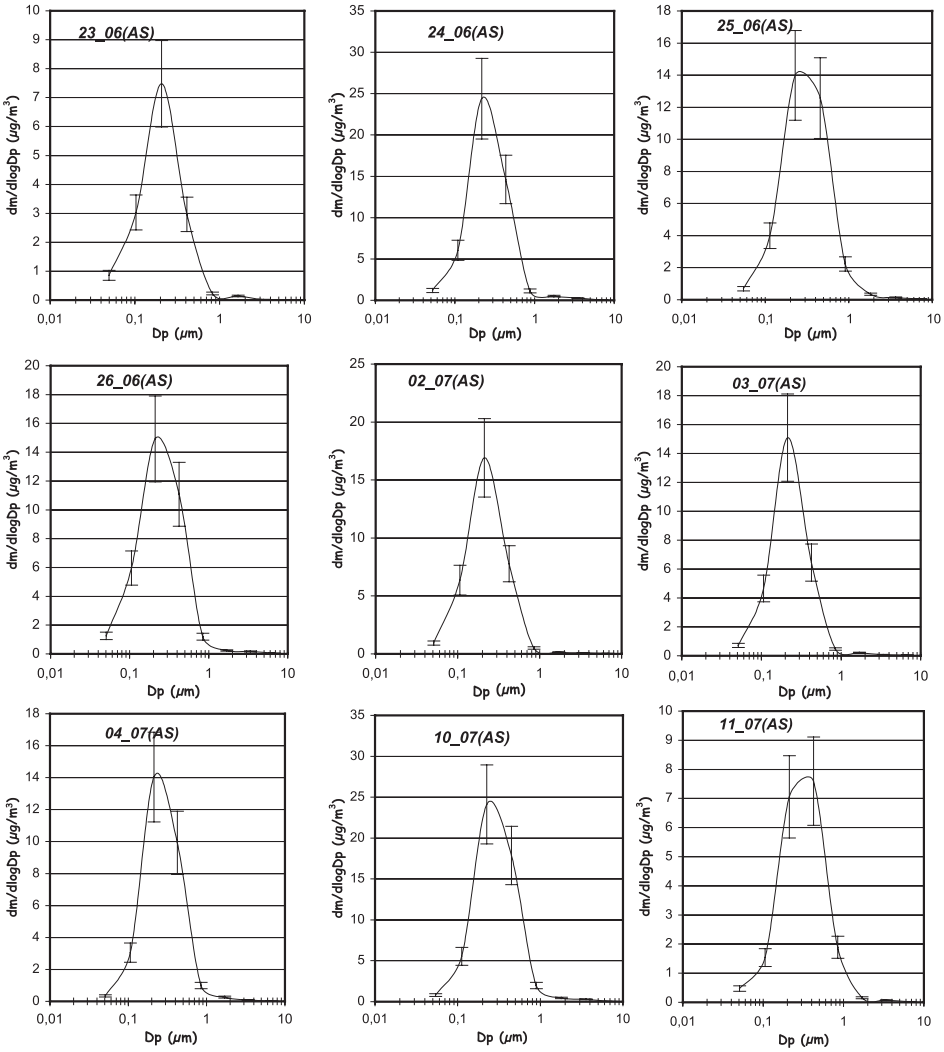

Fig. 2. Ammonium sulfate (AS) mass size distributions in wet state measured during IOPs.

The single scattering albedo has a mean value $\omega_0^{AS} = 0.97 \pm 0.04$ in wet state ($h = 52\%$) and 0.95 ± 0.04 in dry state, indicating the main scattering effect of (AS). The mean asymmetry factor g^{AS} is equal to 0.58 ± 0.04 in wet state and 0.52 ± 0.04 in dry state. This last value is smaller than those generally used in recent radiative forcing simulations of (AS) at global scale. For example, Khiel et al. (2000) and Grant et al. (1999) reported, respectively, g^{AS} equal to 0.66 and 0.65 in dry state. This is probably due to the differences of the lognormal size distribution parameters classically used in dry state to simulate the direct radiative forcing at global scale.

Table 2
Aerosol microphysical properties ($r_{g,n(0)}$, $r_{g,n(h)}$, σ, N) of the number size distribution

Aerosol	Mode		23/06	24/06	25/06	26/06	02/07	03/07	04/07	10/07	11/07	Mean
BC	Fine	$r_{g,n}$	0.017	0.046	0.025	0.019	0.039	0.031	0.037	0.020	0.027	0.028 ± 0.010
		σ	2.07	1.71	1.97	2.03	1.77	1.85	1.82	2.15	1.95	1.94 ± 0.14
		N	3632	675	2731	5170	2156	918	470	2171	954	–
POM	Fine	$r_{g,n(0)}$	0.026	0.036	0.016	0.023	0.015	0.024	0.025	0.042	0.037	0.027 ± 0.010
		$r_{g,n(h)}$	0.029	0.046	0.023	0.027	0.018	0.029	0.031	0.057	0.044	0.034 ± 0.010
		σ	1.76	1.77	2.06	1.98	2.17	1.85	1.82	1.78	1.65	1.86 ± 0.16
		N	6012	1970	8524	7256	8330	5737	4003	710	2003	–
	Accumulation	$r_{g,n(0)}$	0.310	0.223	0.192	0.404	0.437	0.197	0.145	0.305	0.408	0.291 ± 0.100
		$r_{g,n(h)}$	0.330	0.282	0.275	0.473	0.534	0.241	0.177	0.410	0.484	0.364 ± 0.120
		σ	1.90	1.98	2.18	1.84	1.66	2.17	2.20	1.87	1.76	1.95 ± 0.19
		N	0.933	1.29	1.31	0.69	0.612	1.439	2.34	0.87	0.66	–
AS	Fine	$r_{g,n(0)}$	0.034	0.046	0.037	0.034	0.039	0.045	0.048	0.044	0.047	0.040 ± 0.005
		$r_{g,n(h)}$	0.039	0.060	0.048	0.041	0.046	0.056	0.058	0.063	0.055	0.050 ± 0.010
		σ	1.76	1.65	1.78	1.84	1.69	1.63	1.66	1.68	1.78	1.74 ± 0.07
		N	4700	3926	3688	4960	4600	2981	2344	3608	1182	–
N	Accumulation	$r_{g,n(0)}$	0.520	0.508	0.502	0.526	0.518	0.481	0.505	0.463	0.530	0.505 ± 0.020
		$r_{g,n(h)}$	0.595	0.664	0.657	0.624	0.614	0.604	0.616	0.659	0.619	0.628 ± 0.030
		σ	1.62	1.60	1.61	1.64	1.66	1.68	1.57	1.62	1.51	1.61 ± 0.05
		N	0.4	0.68	0.29	0.32	0.31	0.24	0.34	0.48	0.19	–
SS	Accumulation	$r_{g,n(0)}$	0.451	0.340	0.316	0.355	0.314	0.398	0.343	0.285	0.409	0.350 ± 0.050
		$r_{g,n(h)}$	0.515	0.440	0.413	0.421	0.372	0.500	0.418	0.405	0.478	0.440 ± 0.030
		σ	1.69	1.77	1.74	1.78	1.83	1.72	1.75	1.81	1.73	1.75 ± 0.04
		N	0.34	0.81	0.27	0.45	0.41	0.12	0.42	0.67	0.71	–
Dust	Fine	$r_{g,n}$	0.044	0.044	0.011	0.018	0.017	0.030	0.079	0.044	–	0.036 ± 0.010
		σ	2.27	1.57	2.40	2.18	2.15	2.00	1.56	1.67	–	1.97 ± 0.30
		N	180	236	4730	1871	1544	426	225	420	514	–
	Accumulation	$r_{g,n}$	0.554	0.596	0.163	0.365	0.376	0.319	0.264	0.363	–	0.360 ± 0.130
		σ	1.73	1.68	2.37	1.95	1.94	2.06	2.03	1.92	–	1.98 ± 0.21
		N	0.153	0.17	6.11	1.89	0.94	2.38	1.436	1.76	0.57	–

The mean mass extinction efficiency value for the ammonium sulfate (AS) is 2.6 ± 0.5 $m^2\ g^{-1}$ in wet state ($h = 52\%$). Various magnitude of the (AS) mass extinction efficiency have been suggested, but most values at low relative humidity ($h < 60\%$) fall in the range 3.6–7.5 $m^2\ g^{-1}$ (Charlson et al., 1999). Hence, the fact that sulfate are smaller in our study leads to smaller extinction efficiencies. Our value is then more than twice smaller than the classical value of 6.00 $m^2\ g^{-1}$ in wet state ($h = 50\%$) adopted in recent studies (Myhre et al., 1998; Takemura et al., submitted for publication) to simulate the (AS) direct radiative impact at global scale.

4.1.2. Nitrates (N)

While sulfate and ammonium are mainly found in the fine mode, nitrate can be found both in the coarse and in the fine mode (Zhuang et al., 1999). Indeed, coarse nitrate of the mass size distribution has often been observed in coastal areas such as in Finland (Pakkanen, 1996), US (Savoie and Prospero, 1982) or Mediterranean zone (Sellegri et al., 2001).

The (N) mass size distributions obtained during IOPs are reported in Fig. 3. They are unimodal with a coarse mode diameter around 1–2 μm. The (N) mass size distributions indicate clearly that nitrates are mainly found on coarse mode in peri-urban coastal zone during ESCOMPTE.

The corresponding number geometrical radius $r^{N}_{g,n(h)}$ is in the accumulation mode and ranges from 0.595 to 0.659 μm with a mean value equal to 0.628 ± 0.030 μm (Table 2) in wet state and $r^{N}_{g,n(0)} = 0.505 \pm 0.020$ μm in dry state. The associated standard deviation is $\sigma = 1.61 \pm 0.05$.

Although IPCC (2001) identified nitrate aerosol as a significant anthropogenic source of aerosol, very few data concerning its optical properties are available. Our in situ measurements and the use of the complex refractive index of the water-soluble aerosol model (WCP, 1984), allowed us to compute the (N) optical parameters (Table 3). The mean extinction coefficient is equal to 0.002 ± 0.001 km^{-1}, corresponding to $5 \pm 2\%$ of the total extinction (Fig. 8). This indicates the weak contribution of nitrate to the light extinction, mainly due to the presence of (N) on the accumulation mode of the number size distribution in this case, less optically active than the fine mode.

The single scattering albedo has a mean value $\omega_0^{N} = 0.93 \pm 0.04$ in wet state and 0.89 in dry state indicating a none negligible absorption of nitrate aerosol when they are present on the accumulation mode. The mean value of the asymmetry parameter is 0.74 ± 0.04 in wet state and 0.70 ± 0.04 in dry state. This mean value is greater than the computed g^{AS} (0.52), due to the more important forward diffusion of the accumulation mode compared to the fine.

The mass extinction efficiency is equal to 1.24 ± 0.10 $m^2\ g^{-1}$ in wet state indicating that the presence of nitrate on the accumulation mode (associated generally with sea salt) reduces its extinction efficiency because accumulation mode is less efficient, per unit mass, at extinction light.

4.1.3. Black carbon (BC)

Fig. 4 presents the nine (BC) mass size distributions. (BC) particle number size distributions are unimodal with a mean value of the geometrical radius $r^{BC}_{g,n}$ equal to

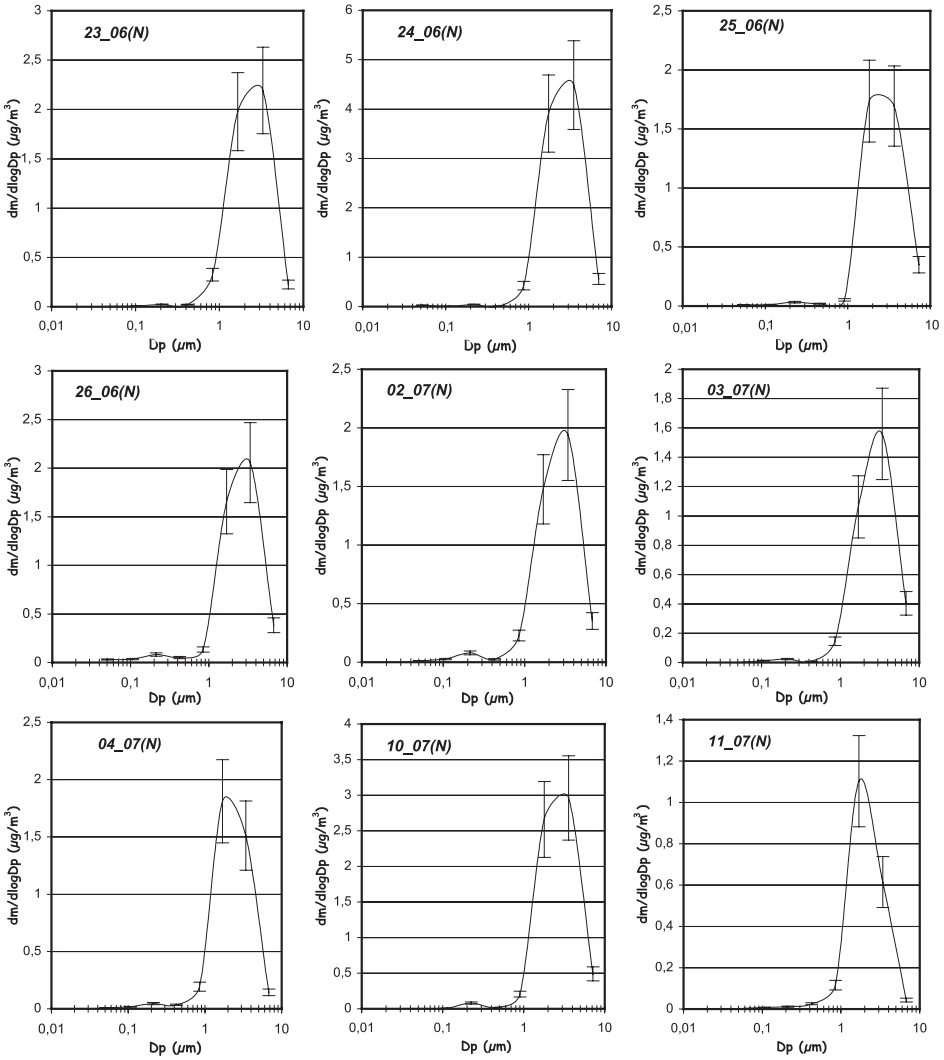

Fig. 3. Nitrate (N) mass size distributions in wet state measured during IOPs.

0.028 ± 0.010 µm (Table 2), and an associated standard deviation $\sigma = 1.94 \pm 0.14$. This $r_{g,n}^{BC}$ is twice larger than that (0.0118 µm) proposed by WCP (1984) and used in numerous simulations of its direct radiative impact at global scale, but is comparable with more recent measurements (Berner et al., 1996; Clarke et al., 1997; Hitzenberg and Tohno, 2001), which reported ($r_{g,n}^{BC}/\sigma$) equal to (0.03 µm/1.7; 0.03 µm/2; 0.035 µm/1.54), respectively.

To calculate the (BC) optical parameters, we used the refractive intermediate value recently proposed by Marley et al. (2001): $m^{BC} = 1.87 - 0.569i$ at 550 nm. Optical computations indicate a mean BC extinction coefficient equal to 0.012 ± 0.004 km^{-1} leading to a mean contribution of $20 \pm 4\%$ (Fig. 8) of the total light extinction. This

Table 3
Aerosol optical properties [K_{ext} (km^{-1}), g, ω_0] at 550 nm in wet state

Aerosol	Mode		23/06	24/06	25/06	26/06	02/07	03/07	04/07	10/07	11/07	Mean
BC	Fine	K_{ext}	0.010	0.015	0.018	0.017	0.010	0.008	0.006	0.012	0.007	0.012 ± 0.004
		g	0.42	0.46	0.44	0.42	0.35	0.43	0.45	0.48	0.45	0.43 ± 0.04
		ω_0	0.31	0.37	0.34	0.31	0.29	0.34	0.36	0.35	0.35	0.33 ± 0.03
POM	Fine	K_{ext}	0.005	0.011	0.012	0.017	0.009	0.008	0.006	0.010	0.006	0.009 ± 0.004
		g	0.46	0.59	0.58	0.58	0.59	0.52	0.52	0.65	0.49	0.59 ± 0.06
		ω_0	0.96	0.98	0.98	0.97	0.97	0.97	0.97	0.98	0.97	0.98 ± 0.01
	Accumulation	K_{ext}	0.002	0.002	0.003	0.003	0.002	0.002	0.002	0.003	0.001	0.002 ± 0.001
		g	0.74	0.74	0.75	0.74	0.72	0.74	0.73	0.75	0.73	0.74 ± 0.01
		ω_0	0.95	0.96	0.95	0.93	0.94	0.94	0.95	0.96	0.93	0.94 ± 0.01
AS	Fine	K_{ext}	0.015	0.038	0.027	0.028	0.021	0.019	0.023	0.043	0.019	0.026 ± 0.010
		g	0.54	0.59	0.61	0.60	0.54	0.55	0.59	0.62	0.63	0.58 ± 0.03
		ω_0	0.96	0.98	0.98	0.97	0.97	0.97	0.97	0.98	0.97	0.97 ± 0.01
N	Accumulation	K_{ext}	0.001	0.004	0.001	0.001	0.001	0.001	0.001	0.002	0.001	0.002 ± 0.001
		g	0.73	0.75	0.75	0.74	0.74	0.75	0.73	0.75	0.72	0.74 ± 0.01
		ω_0	0.91	0.94	0.94	0.92	0.92	0.92	0.93	0.95	0.92	0.93 ± 0.01
SS	Accumulation	K_{ext}	0.001	0.002	0.0001	0.001	0.001	0.0004	0.001	0.002	0.002	0.0010 ± 0.0007
		g	0.72	0.74	0.74	0.73	0.73	0.73	0.73	0.75	0.72	0.73 ± 0.01
		ω_0	0.99	0.99	0.99	0.99	0.99	0.99	0.99	0.99	0.99	0.99 ± 0.01
Dust	Fine	K_{ext}	0.0004	0.0005	0.0032	0.0032	0.0017	0.0021	0.00025	0.0018	0.0016	0.0016 ± 0.0011
		g	0.56	0.56	0.58	0.56	0.56	0.59	0.56	0.50	0.59	0.56 ± 0.03
		ω_0	0.96	0.96	0.96	0.96	0.96	0.96	0.96	0.96	0.96	0.96 ± 0.01
	Accumulation	K_{ext}	0.0006	0.0008	0.0059	0.0049	0.0026	0.0055	0.0022	0.0044	0.0013	0.003 ± 0.002
		g	0.73	0.73	0.71	0.70	0.72	0.72	0.71	0.72	0.72	0.72 ± 0.01
		ω_0	0.88	0.88	0.90	0.89	0.89	0.89	0.91	0.90	0.90	0.89 ± 0.01

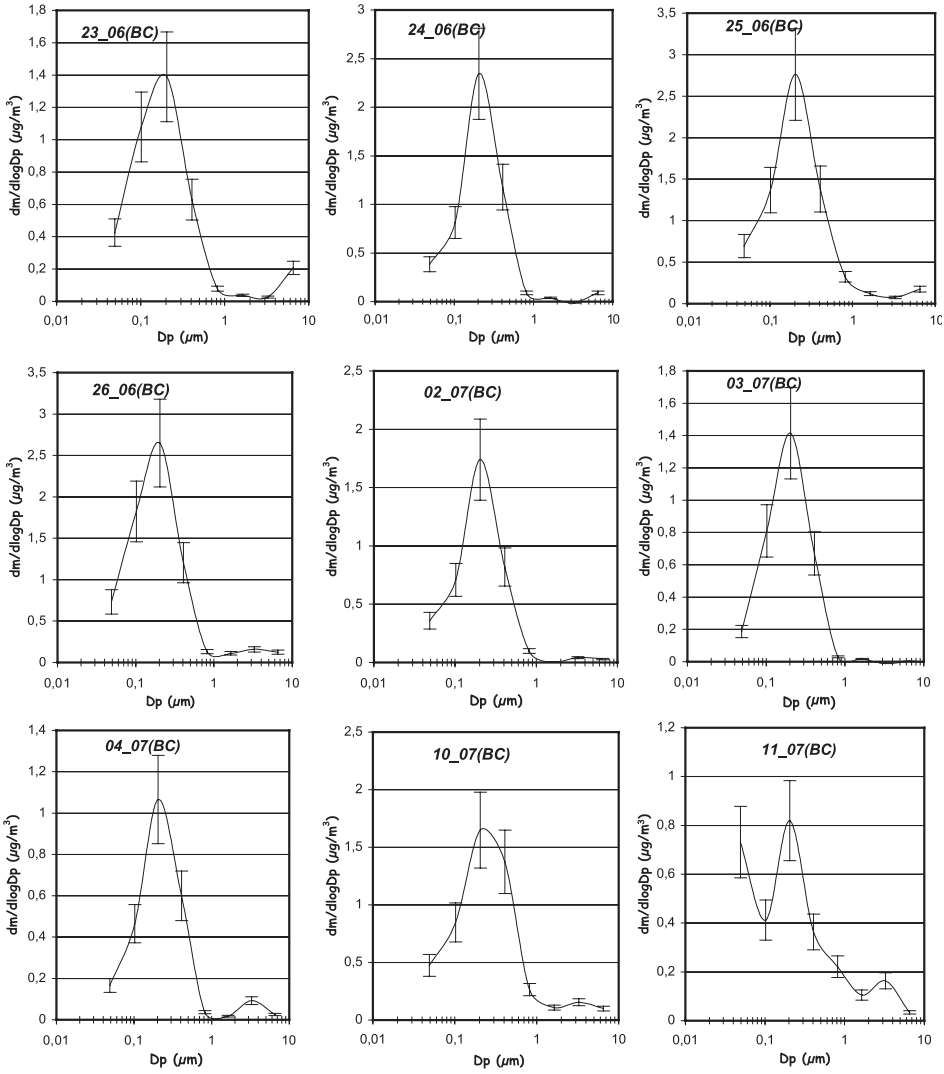

Fig. 4. Black carbon (BC) mass size distributions in wet state measured during IOPs.

illustrates clearly the importance of this aerosol specie which is the second contributor to the light extinction in peri-urban zone. This contribution to extinction is more important than those reported during INDOEX (11%) (Ramanathan et al., 2001) or TARFOX (7%) (Hegg et al., 1997), maybe due to the site of measurements during ESCOMPTE, which was more close to the source of pollution than those used during INDOEX (island of Kaashidhoo, in the Republic of the Maldives, about 500 to 1000 km downwind of major cities in the Indian sub-continent) or TARFOX (North Atlantic off the Eastern coast of the United States).

The single scattering albedo at 550 nm has a mean value $\omega_0^{BC} = 0.33 \pm 0.03$ (Table 3), which is larger than that generally (0.25) used in radiative simulations (Myhre et al., 1998) at global scale and results for the asymmetry factor show a mean value of $g^{BC} = 0.43 \pm 0.04$ which is higher than those (0.33) computed by D'Almeida et al. (1991) indicating a larger scattering of the solar energy in the forward direction.

Finally, the values of the mass specific extinction σ_{ext}^{BC}, vary from 8.00 to 9.65 $m^2\ g^{-1}$ with a mean value around $8.52 \pm 0.48\ m^2\ g^{-1}$. This value fairly agrees with the value of 10 $m^2\ g^{-1}$ generally adopted in many studies in spite of the wide range of observed values: 5–20 $m^2\ g^{-1}$ (Liousse et al., 1993; Martins et al., 1998).

4.1.4. Particulate organic matter (POM)

The (POM) mass size distributions measured during IOPs present a bimodal structure with D_p around 0.22 and 3.45 μm (Fig. 5). Concerning the (POM) accumulation mode (indexed by a), the averaged $r_{g,n(h)}^{POM,a}$ is 0.364 ± 0.120 μm, with a geometric standard deviation equal to 1.95 ± 0.19. The corresponding $r_{g,n(h)}^{POM,f}$ for the fine mode (indexed by f) presents a mean value of 0.034 ± 0.010 μm and a geometric standard deviation around 1.86 ± 0.16 (Table 3) strikingly different from those reported during the Hardiman fire experiment ($r_{g,n(h)}^{POM,f} = 0.08$ μm/$\sigma = 1.7$) . The radius found from our measurements is almost three times smaller, whereas σ is larger. One main reason for this discrepancy might reside in the combustion temperature which is lower for biomass burning, especially in the smoldering step, which produces the biggest particles. Another reason might be the situation of our site where intense production of organic OC took place during IOPs.

Using the complex refractive index $m^{POM} = 1.55 - 0.005i$ at 550 nm proposed by Von Hoyningen-Huene et al. (1998), the optical parameters for (POM) have been computed for the two submicron modes, and then for the total POM size distribution. The fine mode, $K_{ext}^{POM,f} = 0.009 \pm 0.004\ km^{-1}$, contributes for $16 \pm 3\%$ to the light extinction while the accumulation mode ($K_{ext}^{POM,a} = 0.002 \pm 0.001\ km^{-1}$) contributes only for $4 \pm 1\%$. This leads to a global contribution of $20 \pm 4\%$ (Fig. 8) which indicates clearly the important role of POM in the extinction process as shown recently by Hegg et al. (1997) or Novakov et al. (2000).

The computations also show that the (POM) single scattering albedo is almost constant whatever the mode, 0.98 ± 0.01 and 0.94 ± 0.01 for the fine and accumulation modes, respectively (Table 3). These values clearly indicate that the particulate organic matter mainly scatters solar radiation. On the other hand, σ_{ext} and g are different for the two modes. Average values show different behaviour of the two modes as $\sigma_{ext}^{POM,f} = 1.6\sigma_{ext}^{POM,a}$, while $g^{POM,f} = 0.8g^{POM,a}$. Fine mode particles are more efficient for extinction, whereas those of the accumulation mode mainly scatter light in the forward direction.

Concerning the total POM fraction, the mean single scattering albedo value is $\omega_0^{POM} = 0.97 \pm 0.03$. The mean σ_{ext}^{POM} equal to $2.08 \pm 0.3\ m^2\ g^{-1}$ and differs largely from the values computed from the biomass burning experiments (6.00 $m^2\ g^{-1}$) reported by Penner et al. (1999).

Few data on the (POM) microphysical and optical properties are available at present time in the literature and in absence of any good data for describing the size distributions of (POM) from fossil fuel or urban emissions, the size distribution reported by Radke et al.

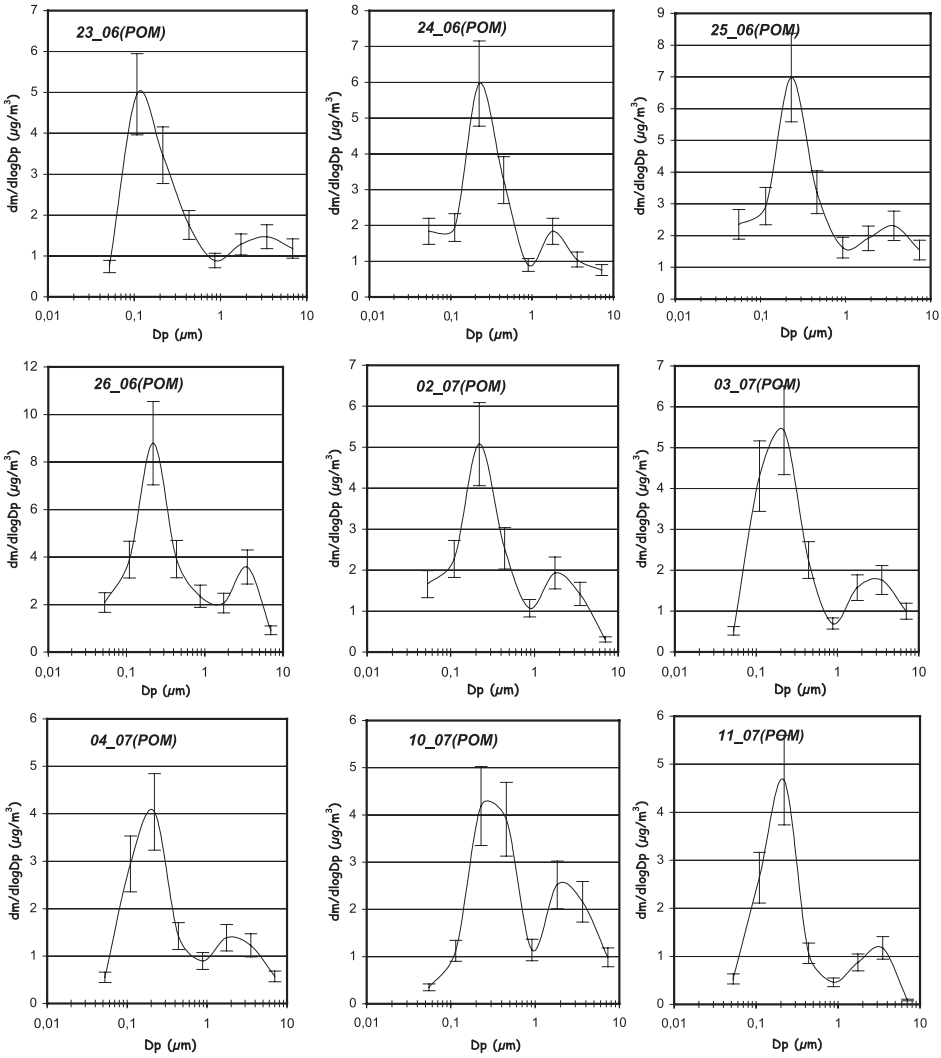

Fig. 5. Particulate organic matter (POM) mass size distributions in wet state measured during IOPs.

(1998) measured during Hardiman Fire experiment is used in radiative simulations to compute the (POM) radiative forcing at global scale (Penner et al., 1998). Although measured at local scale and for special meteorological conditions, ours measurements provide interesting (POM) microphysical and optical properties, produced in large urban areas.

4.1.5. Natural (dust+sea salt) aerosol

Although our study is focusing on the anthropogenic aerosol, we studied the microphysical and optical properties of natural aerosol, including sea salt and dust.

The (D) mass size distributions are reported in Fig. 6. The mass geometrical diameter presents a bimodal structure with D_p around 0.1–0.2 and 2–3 μm, respectively. The corresponding mean fine radius number is $r_{g,n}^{D,f} = 0.036 \pm 0.010$ μm, and the geometric standard deviation is around 1.97 ± 0.30 (Table 2). Although different, our value is coherent with the mineral background nucleation mode (IPCC, 2001) (0.05 μm/2.8). Concerning the accumulation mode, the averaged value gives $r_{g,n}^{D,a} = 0.36 \pm 0.13$ μm, with a geometric standard deviation equal to 1.98 ± 0.21 (Table 2), values which are in good agreement with those reported by Hess et al. (1998) (0.39 μm/2.00).

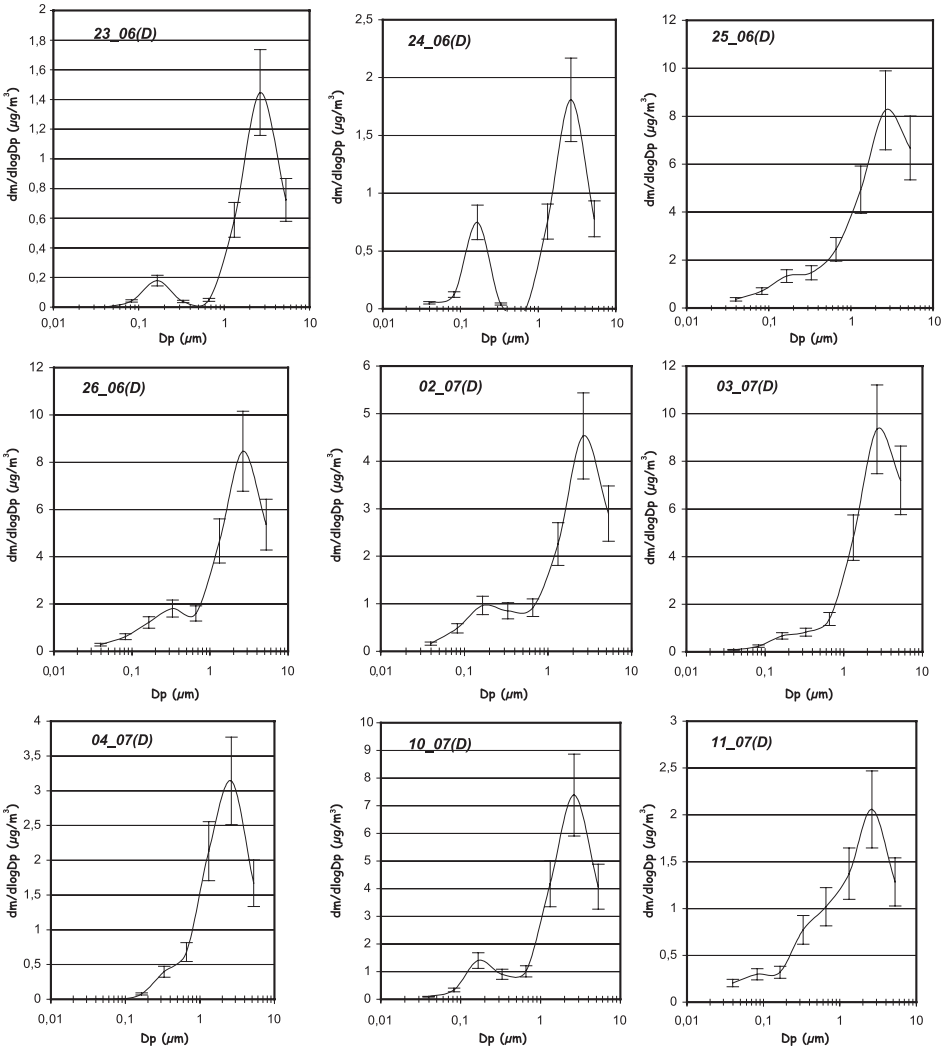

Fig. 6. Mineral aerosol (D) mass size distributions in wet state measured during IOPs.

The optical properties are calculated using the complex refractive index value $1.55 - i5.00 \times 10^{-3}$ used by D'Almeida et al. (1991) in his dust aerosol model. The mean extinction coefficient (Table 3) of the total size distribution is equal to 0.0047 ± 0.0031 km^{-1} and the contribution to the extinction leads to a non-negligible value of $8 \pm 4\%$ (Fig. 8).

Concerning the sea salt fraction, the (SS) mass size distributions obtained are reported in Fig. 7. They are unimodal with a coarse mode diameter around 1–2 μm. The corresponding number geometrical radius $r^{SS}_{g,n(h)}$ ranges equal to 0.440 ± 0.030 μm (Table 2), and the associated standard deviation is $\sigma = 1.75 \pm 0.04$.

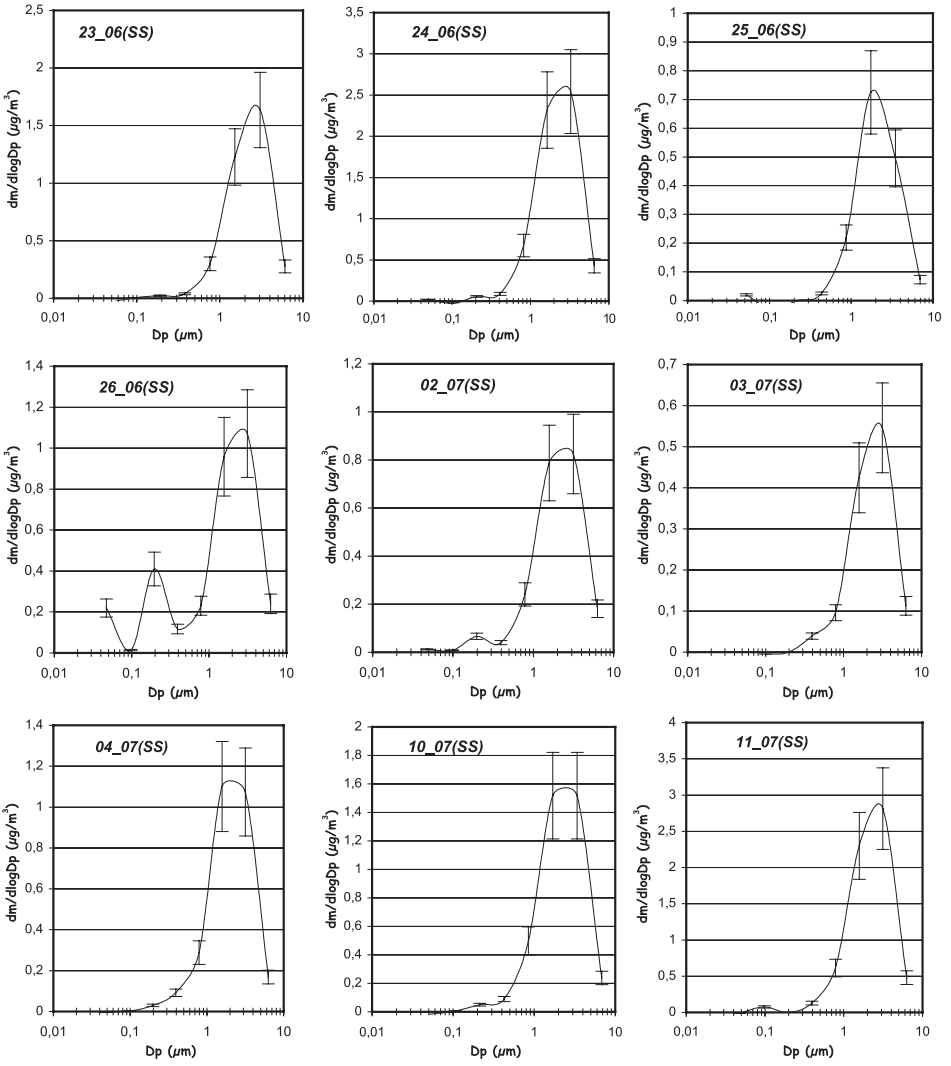

Fig. 7. Sea salt (SS) mass size distributions in wet state measured during IOPs.

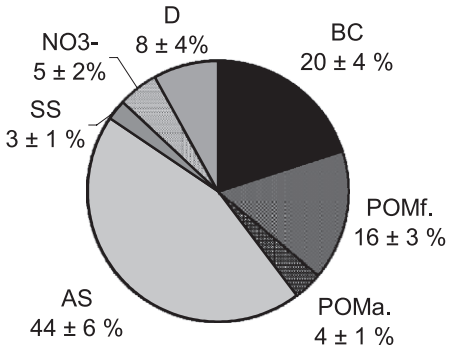

Fig. 8. Contribution to the light extinction at 550 nm of each aerosol species.

To compute the optical properties, we used the refractive index used in the oceanic model by D'Almeida et al. (1991): $m^{SS} = 1.50 - 2.10^{-8}i$, in dry state. Results show a slightly contribution of (SS) to the light extinction in peri-urban zone, with an average contribution of only $3 \pm 1\%$ (Fig. 8).

5. Optical properties of the total aerosol layer and comparisons with AERONET inversions

In order to validate our computations, we compared the optical properties of the total aerosol population measured in situ, at ground level, with information available from measurements of the CIMEL photometer. Two hypotheses must first be made. One concerns the type of mixture of the particles: internal or external. According to previous study by Covert and Heintzenberg (1984) or more recently by Hasegawa and Ohta (2002), aerosol particles exhibited a large and predominant degree of external mixture near an urban source region. Hence, we considered that the particles were, in our situation, externally mixed. Then the whole population of the aerosol particles is considered as the sum of the contributions of the different components (see below).

The second hypothesis concerns the representativity of measurements made in situ, near ground level, with respect to information concerning the total atmospheric column, furnished by the CIMEL photometer. During the ESCOMPTE experiment, the aerosol concentrations profiles recorded during the ARAT aircraft flights indicated that aerosol were mainly confined in the PBL which is close to 1 km, as shown in Fig. 9. The records of the potential temperature profiles (Fig. 9) showed, for all the days studied, a positive gradient indicating a PBL stable and well homogenized. Furthermore, the Angström coefficient $\alpha_{440/670}$ is comprised between 1.10 and 1.82 for all the days studied. This implies that the extinction is mainly due to submicronic anthropogenic aerosol (Liousse et al., 1995) and shows, at least, that any dust events were found during the ESCOMPTE experiment. Hence, we assumed that the ground based aerosol optical characterization was representative of the entire aerosol layer mainly confined in the PBL, and might be compared with the AERONET retrievals.

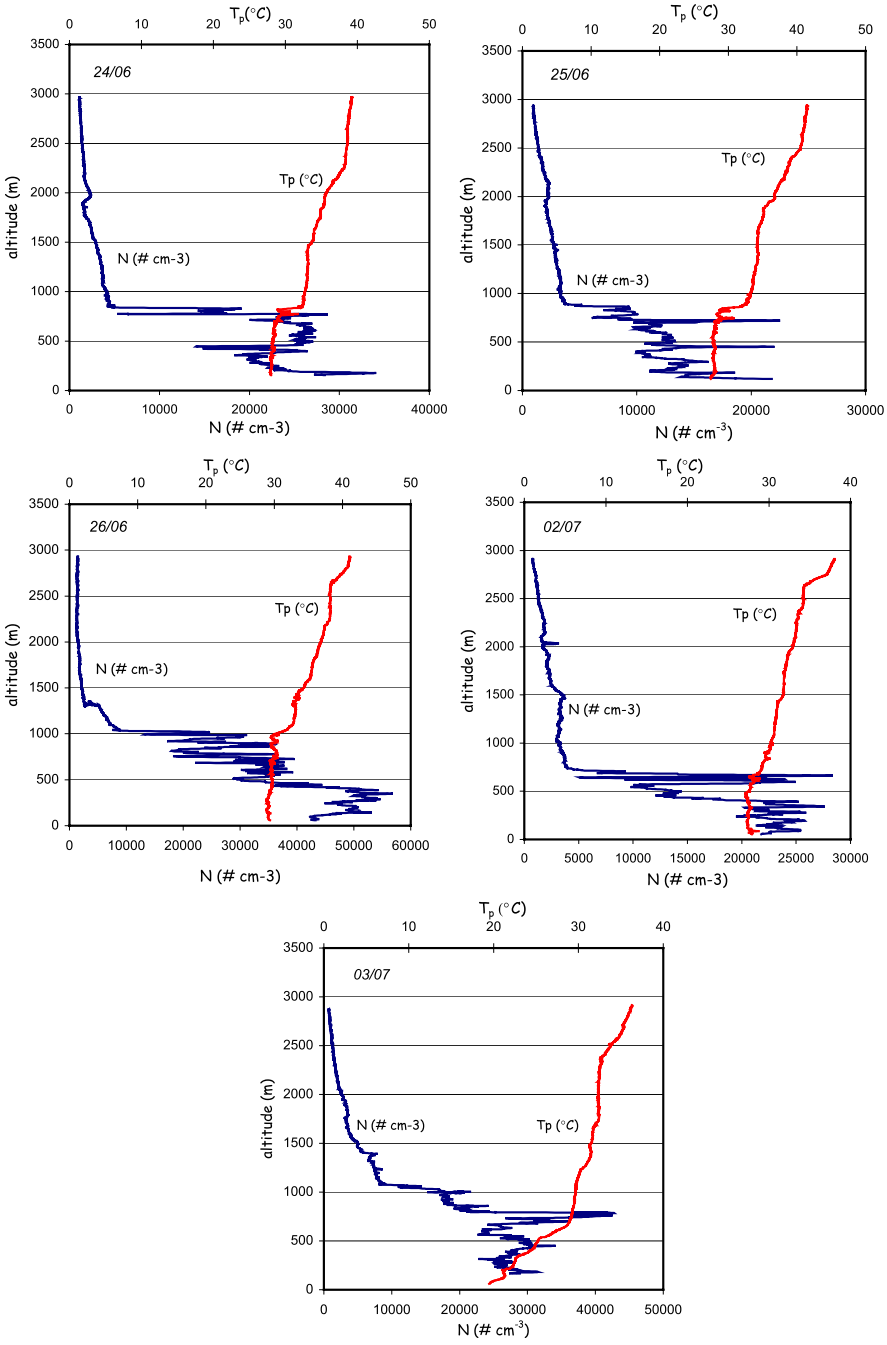

Fig. 9. Number concentrations and potential temperature profiles.

Table 4
Asymmetry parameter for the total aerosol population, in wet state, at 550 nm

Date	23/06	24/06	25/06	26/06	02/07	03/07	04/07	10/07	11/07	Mean
g^t	0.55	0.60	0.61	0.59	0.57	0.57	0.59	0.63	0.60	0.59 ± 0.05

5.1. Asymmetry and single scattering albedo parameters

The asymmetry parameter and the single scattering albedo for the total aerosol population, g^t and ω_0^t are computed as follows:

$$g^t = \frac{\sum_i K_{\mathrm{diff},i} \times g_i}{\sum_i K_{\mathrm{diff},i}} \tag{7}$$

$$\omega_0^t = \frac{\sum_i K_{\mathrm{ext},i} \times \omega_{0,i}}{\sum_i K_{\mathrm{ext},i}} \tag{8}$$

where g_i, $K_{\mathrm{diff},i}$, $K_{\mathrm{ext},i}$ and $\omega_{0,i}$ are, respectively, the asymmetry parameter, the scattering coefficient, the extinction coefficient and the single scattering albedo of each aerosol species i. The values of g^t are reported in Table 4 for each day. The mean value is 0.59 ± 0.05. Few values of g are reported in the literature in urban coastal atmosphere from in situ measurements. However, it must be noted that our value agrees well with g computed from data of Chazette and Liousse (2001) on Thessaloniki (coastal city) in Greece (0.61) ($h = 45\%$) or for an old anthropogenic aerosol from the Northeast US coast and transported to the Western Atlantic (0.58) (Hignett et al., 1999) during TARFOX. Those two last values were obtained by measuring the size distribution and assessing the complex refractive index from aerosol chemical analysis. At the Goa coastal city in India during INDOEX, Leon et al. (2002) reported a value of 0.53, computed from optical measurements.

Values of ω_0^t (see Table 5) indicate a mean value of 0.85 ± 0.05 in wet state. This result indicates an important absorption of the solar radiation on the Vallon d'Ol site during the pollution events studied here. Our value is comparable with ω_0 reported in other coastal urban atmosphere (see Table 6) experiments. Chazette and Liousse (2001) reported (0.82) ($h = 45\%$) and Alfaro et al. (submitted for publication) reported (0.89) for the Goa city during INDOEX. For pure urban atmosphere (see Table 6), Bergin et al. (2001) reported

Table 5
Single scattering albedo for the total aerosol population, in wet state, at 550 nm

Date	23/06	24/06	25/06	26/06	02/07	03/07	04/07	10/07	11/07	Mean
ω_0^t	0.79	0.86	0.81	0.81	0.83	0.85	0.88	0.88	0.85	0.85 ± 0.05

Table 6
ω_0 computed in coastal urban or pure urban atmosphere in wet state ($h \approx 50\%$) at 550 nm

Urban atmosphere				
	ESCOMPTE	Mexico	Thessaloniki	Beijing
ω_0	0.85	0.80–0.88	0.82	0.81

(0.81) on Beijing ($30\% < h < 70\%$) and a recent study carried out on Mexico City using nephelometer and aethalometer measurements, indicates a value comprised between $0.80 \leq \omega_0 \leq 0.88$ (Baumgardner et al., 2000). Hence, at it was the case for the asymmetry parameter, our computations seem to be coherent with other in situ measurements made in urban coastal or pure urban atmosphere.

5.2. Comparison with AERONET inversions

The accuracy of individual aerosol property retrievals by the (Dubovik and King, 2000) method from the measurements of CIMEL radiometers (performed under AERONET-standardized protocol of instrument maintenance and data processing) where analyzed in extensive sensitivity simulations (Dubovik et al., 2000). The analysis showed that an accurate ω_0 and g retrieval (with accuracy to the level of 0.03) can be retrieved for high aerosol loading ($\delta_a(440) \geq 0.4$) and for solar zenith angle $\geq 50°$.

During ESCOMPTE, 6 days (24th, 25th, 26th of June and 02nd, 03rd, 04th of July) agree with these conditions and allowed us to compare the optical properties computed from in situ measurements and retrieved by AERONET. The AERONET retrieval are made at 440 and 670 nm for short wavelength (SW), hence the value at 550 nm have been computed by interpolation between the values at 440 and 670 nm.

Concerning the single scattering albedo (Table 7), good agreements are observed. The mean value during the ESCOMPTE experiment computed in situ agrees with the AERONET retrieval ($\omega_0^{\text{in situ}} = 0.83/\omega_0^{\text{AER}} = 0.86$) in wet state. Furthermore, results presented in Table 3 indicate relatively good agreements for all the days studied except for the 25th where $\omega_0^{\text{in situ}} = 0.81$ and $\omega_0^{\text{AER}} = 0.89$. This agreement is coherent with previous comparisons reported in Dubovik et al. (2002) where independent in situ measurements of ω_0 during TARFOX (Hegg et al., 1997) (0.95) or during the INDOEX experiment (Eck et al., 2001) (0.86–0.90) showed reasonable agreements with AERONET retrievals.

Table 7
Comparison between AERONET and in situ aerosol optical properties at 550 nm

Event	Date	ω_0^{AER}	$\omega_0^{\text{in situ}}$	g^{AER}	$g^{\text{in situ}}$
1	June 24	0.85	0.86	0.63	0.60
2	June 25	0.89	0.81	0.64	0.61
3	June 26	0.85	0.81	0.67	0.59
4	July 02	0.87	0.84	0.62	0.58
5	July 03	0.84	0.85	0.65	0.57
6	July 04	0.89	0.88	0.64	0.59
Mean		0.86	0.84	0.64	0.59

While some studies were dedicated to study ω_0 in urban atmosphere, few studies were carried out to estimate g and compare it with AERONET retrieval. In contrary to ω_0, the mean g retrieved from AERONET is slightly higher than g computed in situ ($g^{\text{in situ}} = 0.59 \pm 0.04/g^{\text{AER}} = 0.64 \pm 0.04$) (see Table 7). We note the same tendency for all the days studied as it is shown in Table 7. Indeed, (except for the 26th of June and the 03rd of July where significant differences appear), the asymmetry parameters computed are 10% lower than the AERONET retrievals, but remain coherent within the uncertainty levels of the AERONET and in situ retrievals of g (± 0.05). These differences could also be explained by an under estimation of the coarse mode measured in situ. Indeed, it is less stable (in time and in space) than the fine (accumulation) mode and many factors can result to miss sampling. The sampling of coarse aerosols is often a limitation in computing scattering from in situ data (Quinn and Coffman, 1998). Hence, we consider that the results deduced from the two techniques of measurements are in a rather good agreement.

6. Discussion

Even if the results obtained are deduced from local and in situ measurements, and often quite different from those yet published (AS, N, BC and POM microphysics and optical properties) and generally used in global models, we think that they are well representative of a urban zone in conditions of pollution events. Indeed, it must be noted here that the 9 days studied correspond to similar meteorological conditions characterized by anticyclonic conditions, clear sky, low wind breeze and high temperatures favouring accumulation of pollutants in the PBL and photochemical effects leading to elevated levels of ozone formation, between 80 and 150 ppb, in different points of the experimental domain (Cros et al., submitted for publication). On the other hand, the optical parameters values g, ω_0 and σ_{ext} are remarkably constant for each specie and all day(s), as showed by the low values of the standard deviations with respect to the average values calculated, comprised between 1% and 11% only (see Table 3). So, we may assume that these values are characteristics of each component (specie) in that situation of pollution event in urban and near urban zones. Consequently, we may also assume that, when they are different from those already published, the difference is significative and among these differences, those concerning the BC and POM properties must be highlighted.

It appears difficult to use our measurements in recent models which cannot represent the near-urban environment because a typical size of a grid square is 5° by 5°. However, the microphysical and optical properties we report here should be of interest for the urban and near-urban environment modeling and could be used both in radiative forcing studies at meso-scale including urban zone or at global scale as soon as the models could take into account urban emissions with more fine resolution.

7. Conclusion

Microphysical and optical properties of the main aerosol species [ammonium sulfate (AS), nitrate (N), black carbon (BC), particulate organic matter (POM), sea salt (SS) and

mineral aerosol (D)] have been investigated in peri-urban zone during the ESCOMPTE experiment, which took place in South of France during the summer 2001. Aerosol size distributions of each aerosol species, associated with their complex refractive index were used to compute, from the Mie Theory, the key radiative parameters generally used to simulate the direct radiative forcing of aerosol, as the extinction coefficient K_{ext}, the mass extinction efficiency σ_{ext}, the single scattering albedo ω_0 and the asymmetry parameter g at the wavelength of 550 nm and in wet state.

Optical computations indicate clearly that 90% of the light extinction is due to anthropogenic aerosol (AS, N, BC, POM) and 10% is due to natural aerosol (D and SS). The major contributor to the light extinction is (AS) but results indicate clearly the important rule of carbonaceous particles which contribute to 40% of the light extinction. Nitrate (N) has, in this case, a weak contribution to extinction (5%) mainly due to the presence of nitrate aerosol on the coarse mode, less optically active than the fine mode.

Optical computations indicate also that the microphysical and optical properties of the anthropogenic aerosol are often quite different from those yet published (AS, N, BC and POM microphysics and optical properties) and generally used in global models. For example, the (AS) mean specific mass extinction presents a large difference with the value classically adopted at low relative humidity ($h < 60\%$) (2.6 instead of 6 $m^2\ g^{-1}$ at 550 nm).

Optical properties of each aerosol species are used to compute the optical properties of the total aerosol layer, including all aerosol species in external mixture. The single scattering albedo has a mean value of 0.85 ± 0.05 in wet state, indicating an important absorption of solar radiation by the atmospheric layer and the asymmetry parameter has a mean value of 0.59 ± 0.05. The asymmetry parameter and the single scattering albedo computed are found to be coherent with other values reported in aerosol coastal zone. Furthermore, to validate our computations, the AERONET retrievals are used and good agreements are found for the mean single scattering albedo and the asymmetry parameter in wet state.

The microphysical and optical aerosol properties we reported here are representative of an urban zone during strong pollution events and should present some interest in order to study the direct radiative impact of urban aerosol pollution in mesoscale or global models.

Acknowledgements

The authors are indebted to Dr. Bernard Cros and Dr. Pierre Durand for the organization of ESCOMPTE experiment. They gratefully thank the different Institutes in France (CNRS, INSU, ADEME, Ministry of Environment) for their support. Logistic help from local agencies (AIRMAREX and AIRFOBEP) is gratefully acknowledged. We also thank the AERONET staff for the data collection, calibration and processing. We would also like to thank especially the AERONET PI's during ESCOMPTE: Tanré, D. and Blarel, L.

References

Ackerman, A.S., Toon, O.S., Stevens, D.E., Heymsfield, A.J., Ramanathan, V., Welton, E.J., 2000. Reduction of tropical cloudiness by soot. Science 288, 1042–1047.

Alfaro, S., Gomes, L., Gaudichet, A., Rajot, J.L., Leon, J.-L., Cachier, H., Chazette, P., Dulac, F., Sarode, P.R.,

Inamdar, S.R., Kadadevarmath, J.S., 2003. Aerosol model derived from measurements performed at an Indian coastal site during the intensive field phase: size distribution and composition. J. Geophys. Res. (submitted for publication).

Angström, A., 1964. The parameters of atmospheric turbidity. Tellus 16, 64–75.

Bates, T.S., Huebert, B.J., Gras, J.L., Griffiths, F.B., Durkee, P.A., 1998. International Global Atmospheric Chemistry (IGAC) Project's First Aerosol Characterization Experiment (ACE 1): overview. J. Geophys. Res. 103, 16297–16318.

Baumgardner, D.G., Raga, G.B., Kok, G., Ogren, J., Rosas, I., Baez, A., Novakov, T., 2000. On the evolution of aerosols properties at a mountain site above Mexico City. J. Geophys. Res. 105, 22243–22253.

Bergin, M.H., Cass, G.R., Xu, J., Fang, C., Zeng, L.M., Yu, T., Salmon, L.G., Kiang, C.S., Tang, X.Y., Zhang, Y.H., Chameides, W.L., 2001. Aerosol radiative, physical, and properties in Beijing during June, 1999. J. Geophys. Res. 106, 17969–17980.

Berner, A., Sidla, S., Galambos, Z., Hitzenberg, R., 1996. Modal character of atmospheric black carbon size distributions. J. Geophys. Res. 101, 19559–19565.

Cachier, H., Brémond, M.-P., Buat-Ménart, P., 1989. Determination of atmospheric soot carbon with a simple thermal method. Tellus 41B, 379–390.

Charlson, R.J., Anderson, T.L., Rodhe, H., 1999. Direct climate forcing by anthropogenic aerosols: quantifying the link between atmospheric sulfate and radiation. Contrib. Atmos. Phys. 72, 79–94.

Chazette, P., Liousse, C., 2001. A case study of optical and chemical ground apportionment for urban aerosols in Thessaloniki. Atmos. Environ. 35, 2497–2506.

Clarke, A.D., Uehara, T., Porter, J.N., 1997. Atmospheric nuclei and related aerosol fields over the Atlantic: clean subsiding air and continental pollution during ASTEX. J. Geophys. Res. 102, 25281–25292.

Covert, D.S., Heintzenberg, J., 1984. Measurements of the degree of internal/external mixing of hygroscopic compounds and soot in atmospheric aerosols. Sci. Total Environ. 36, 347–352.

Cros, B., Durand, P., Caccia, J.-L., Drobinski, P., Godet, Y., Kottmeier, C., Laverdet, G., Lohou, F., Masclet, P., Ponche, L., Wortham, H., 2003. An overview of the ESCOMPTE Campaign. Atmos. Res. (submitted for publication).

D'Almeida, G.A., Koepke, P., Shettle, E.P., 1991. Atmospheric Aerosols: Global Climatology and Radiative Characteristics. A. Deepak Publishing. 561 pp.

Dubovik, O., King, M.D., 2000. A flexible inversion algorithm for retrieval of aerosol optical properties from Sun and sky radiance measurements. J. Geophys. Res. 105 (D16), 20673–20696.

Dubovik, O., Smirnov, A., Holben, B.N., King, M.D., Kaufman, Y.J., Eck, T.F., Slutsker, I., 2000. Accuracy assessments of aerosol optical properties retrieved from AERONET sun and sky-radiance measurements. J. Geophys. Res. 105, 9791–9806.

Dubovik, O., Holben, B.N., Eck, T.F., Smirnov, A., Kaufman, Y.J., King, M.D., Tanré, D., Slutsker, I., 2002. Variability of absorption and optical properties of key aerosol types observed in worldwide locations. J. Atmos. Sci. 59, 590–608.

Eck, T.F., Holben, B.N., Dubovik, O., Smirnov, A., Slutsker, I., Lobert, J.M., Ramanathan, V., 2001. Column integrated aerosol optical properties over the Maldives during the northeast monsoon for 1998–2000. J. Geophys. Res. 106, 28555–28566.

Grant, K.E., Chuang, C.C., Grossman, A.S., Penner, J.E., 1999. Modeling the spectral optical properties of ammonium sulfate and biomass burning aerosols: parameterization of relative humidity effects and model results. Atmos. Environ. 33, 2603–2620.

Hänel, G., 1976. The properties of atmospheric particles as functions of the relative humidity at thermodynamic equilibrium with surrounding moist air. Adv. Geophys. 19, 73–188.

Hartley, W.S., Hobbs, P.V., Ross, J.L., Russel, P.B., Livingston, J.M., 2000. Properties of aerosols aloft relevant to direct radiative forcing off the mid-Atlantic coast of the United States. J. Geophys. Res. 105, 9859–9885.

Hasegawa, S., Ohta, S., 2002. Some measurements of the mixing state of soot-containing particles at urban and non-urban sites. Atmos. Environ. 36, 3899–3908.

Haywood, J.M., Shine, K.P., 1997. Multi-spectral calculations of the direct radiative forcing of tropospheric sulfate and soot aerosols using a column model. Q. J. R. Meteorol. Soc. 123, 1907–1930.

Hegg, A.D., Livingston, J., Hobbs, P.V., Novakov, T., Russel, P., 1997. Chemical apportionment of aerosol column optical depth off the mid-Atlantic coast of the United States. J. Geophys. Res. 102, 25293–25303.

Hering, S.V., Eldering, A., Seinfeld, J.H., 1997. Bimodal character of accumulation mode aerosol distributions in Southern California. Atmos. Environ. 31, 1–11.

Hess, M., Koepke, P., Schult, I., 1998. Optical properties of aerosols and clouds: the software package. Bull. Am. Meteorol. Soc. 79, 831–844.

Hignett, P., Taylor, J.T., Francis, P.N., Glew, M.D., 1999. Comparison of observed and modelled direct forcing during TARFOX. J. Geophys. Res. 104, 2279–2287.

Hitzenberg, R., Tohno, S., 2001. Comparison of black carbon (BC) aerosols in two urban areas concentrations and size distributions. Atmos. Environ. 35, 2153–2167.

Intergovernment Panel on Climate Change, 2001. In: Houghton, J.T., et al. (Eds.), Climate Change. Cambridge Univ. Press, New York.

Khiel, J.T., Scneider, T.L., Rasch, P.J., Barth, M.C., Wong, J., 2000. Radiative forcing due to sulphate aerosols from simulations with the NCAR community model (CCM3). J. Geophys. Res. 105, 1441–1458.

Leon, J.-F., Chazette, P., Pelon, J., Dulac, F., Randriamarisoa, H., 2002. Aerosol direct radiative forcing impact over the INDOEX area based on active and passive remote sensing. J. Geophys. Res. 107 (D19). (doi:10.1029/2000JD000116)

Liousse, C., Cachier, H., Jennings, S.G., 1993. Optical and thermal measurements of black carbon content in different environments: variation of specific attenuation cross-section, σ. Atmos. Environ., A 27, 1203–1211.

Liousse, C., Devaux, C., Dulac, F., Cachier, H., 1995. Aging of savanna biomass burning aerosols: consequences of their optical properties. J. Atmos. Chem. 22, 1–17.

Liousse, C., Penner, J.E., Chuang, C., Walton, J.J., Eddleman, H., Cachier, H., 1996. A global three-dimensional model study of carbonaceous aerosols. J. Geophys. Res. 101, 19411–19432.

Marley, N.A., Gaffney, S.G., Baird, J.C., Blazer, C.A., Drayton, P.J., Frederick, J.E., 2001. An empirical method for the determination of the complex refractive index of size-fractionated atmospheric aerosols for radiative transfer calculations. Aerosol Sci. Technol. 34, 535–549.

Martins, J.V., Hobbs, P.V., Weiss, R.E., Artaxo, P., 1998. Sphericity and morphology of smoke particles from biomass burning in Brazil. J. Geophys. Res. 103, 32051–32067.

Mie, G., 1908. Beiträge zur Optick trüber medien, speziell kolloidaler Metallösungen. Ann. Phys. (Leipz.) 25, 377–445.

Myhre, G., Stordal, F., Restad, K., Isaksen, I.S.A., 1998. Estimation of the direct radiative forcing due to sulfate and soot aerosols. Tellus, Ser. B 50, 463–477.

Novakov, T., Bates, T.S., Quinn, P.K., 2000. Shipboard measurements of concentrations and properties of carbonaceous aerosols during ACE-2. Tellus 52B, 228–238.

Pakkanen, T.A., 1996. Study of the formation of coarse particle nitrate aerosol. Atmos. Environ. 30, 2475–2482.

Penner, J.E., Chuang, C.C., Grant, K., 1998. Climate forcing by carbonaceous and sulfate aerosols. Clim. Dyn. 14, 839–851.

Penner, J.E., Chuang, C.C., Grant, K., 1999. Climate Change and Radiative Forcing by Anthropogenic Aerosols: A Review of Research During the Last Five Years. The Institute for Advanced Physics Studies, La Jolla, CA, USA.

Putaud, J.P., et al., 2000. Chemical mass closure and assessment of the origin of the submicron aerosol in the marine boundary layer and the free troposphere at Tenerife during ACE-2. Tellus 52B, 141–168.

Quinn, P.K., Coffman, D.J., 1998. Local closure during the First Aerosol Characterization Experiment (ACE1): aerosol mass concentration and scattering and backscattering coefficients. J. Geophys. Res. 103, 15575–15596.

Radke, L.F., Hegg, D.A., Lyons, J.H., Brock, C.A., Hobbs, P.V., Weiss, R., Rasmussen, R., 1998. Airborne measurements on smokes from biomass burning. In: Hobbs, P.V., McCormick, M.P. (Eds.), Aerosols and Climate. A. Deepak Publishing, Hampton, VA, pp. 411–422.

Raes, F., Bates, T., McGovern, F., VanLiedekerke, M., 2000. The 2nd Aerosol Characterization Experiment (ACE-2): general overview and main results. Tellus 52B, 111–125.

Raga, G.B., Castro, T., Baumgardner, D., 2001. The impact of megacity on local climate and implications for the regional environment: Mexico City. Atmos. Environ. 35, 1805–1811.

Ramanathan, V., et al., 2001. Indian experiment: an integrated assessment of the climate forcing and effects of the great Indo-Asian haze. J. Geophys. Res. 106 (D22), 28371–28398.

Rosenfeld, D., 2000. Suppression of rain and snow by urban and industrial air pollution. Science 287, 1793–1796.

Savoie, D.L., Prospero, J.M., 1982. Particle size distribution of nitrate and sulfate in the marine atmosphere. Geophys. Res. Lett. 9, 1207–1210.

Seinfeld, J.H., Pandis, S.N., 1998. From Air Pollution to Climate Change. Atmospheric Chemistry and Physics. Wiley, New York, p. 126.

Sellegri, K., Gourdeau, J., Putaud, J.P., Despiau, S., 2001. Chemical composition of marine aerosol in a Mediterranean coastal zone during the FETCH experiment. J. Geophys. Res. 106 (D11), 12023–12037.

Stern, A.C., 1977. Air Pollution, 3rd ed., vol. IV. Academic Press, New York, p. 103.

Takemura, T., Nakajima, T., Dubovik, O., Holben, B.N., Kinne, S., 2003. Single scattering albedo and radiative forcing of various aerosol species with a global three-dimensional model. J. Clim. 15, 333–352.

Von Hoyningen-Huene, W., Schmidt, T., Chan, A.K., Heintzenberg, J., Neususess, C., 1998. Climate relevant aerosol parameters of South-East-Asian forest fire haze. J. Aerosol Sci. 29, 1259–1260.

WCP, 1984. World Climate Programme. In: McClatchey, R.A., Bolle, H.-J., Kondratyev, K.Ya. (Eds.), A Preliminary Cloudless Standard Atmosphere for Radiation Computation. Int. Radiation Com., Boulder, CO, USA, p. 53.

Whitby, K.T., 1978. On a multimodal nature of atmospheric size distribution. III Int., Conf. on Nucleation, Leningrad, URSS.

Zhuang, H., Chan, C.K., Ming, F., Wexler, A.S., 1999. Size distributions of particulate sulfate, nitrate, and ammonium at a coastal site in Hong Kong. Atmos. Environ. 33, 843–853.